THE JOURNAL OF PHYSICAL CHEMISTRY A LETTERS

2005, *109,* 7839−7842
Published on Web 08/12/2005

Vibrationally Mediated Photodissociation of Ethylene Cation by Reflectron Multimass Velocity Map Imaging

Myung Hwa Kim,[†,‡] Brian D. Leskiw,[†] and Arthur G. Suits*[,†,‡]

Department of Chemistry, Wayne State University, Detroit, Michigan 48202, and Department of Chemistry, SUNY Stony Brook, Stony Brook, New York 11794

Received: June 10, 2005; In Final Form: July 20, 2005

A new imaging technique, reflectron multimass velocity map ion imaging, is used to study the vibrationally mediated photodissociation dynamics in the ethylene cation. The cation ground electronic state is prepared in specific vibrational levels by two-photon resonant, three-photon ionization via vibronic bands of (π, nf) Rydberg states in the vicinity of the ionization potential of ethylene, then photodissociated through the ($\tilde{B}\ ^2A_g$) excited state. We simultaneously record spatially resolved images of parent $C_2H_4^+$ ions as well as photofragment $C_2H_3^+$ and $C_2H_2^+$ ions originating in dissociation from the vibronic excitations in two distinct bands, $7f\ 4_0^2$ and $8f\ 0_0^0$, at roughly the same total energy. By analyzing the images, we directly obtain the total translation energy distributions for the two dissociation channels and the branching between them. The results show that there exist differences for competitive dissociation pathways between H and H_2 elimination from $C_2H_4^+$ depending on the vibronic preparation used, i.e., on the vibrational excitation in the ground state of the cation prior to photodissociation. Our findings are discussed in terms of the possible influence of the torsional excitation on competition between direct dissociation, isomerization, and radiationless transitions through conical intersections among the numerous electronic states that participate in the dissociation.

The vibrationally mediated photodissociation technique developed by Crim and co-workers[1] is a powerful tool to control unimolecular reaction dynamics and probe features of the ground and excited potential energy surfaces. The approach uses excitation of a well-characterized vibrational state, relying upon Franck−Condon factors and energetics to access and explore distinct regions of the excited-state surfaces. Anderson and co-workers have extensively investigated the effects of mode-selective vibrational excitation of polyatomic cations for reaction with neutral molecules, such as $C_2H_2^+ + D_2$, using a resonance-enhanced multiphoton ionization (REMPI) process for state preparation.[2] Very recently, velocity ion map imaging[3] and slice imaging techniques[4−6] combined with REMPI have been successfully applied to study in detail the photodissociation dynamics of the state-selected molecular ions such as Br_2^+,[7] CF_3I^+,[8] $BrCl^+$,[9] and OCS^+.[6] In these experiments, a parent ion is initially created in a single, well-defined electronic, spin−orbit, and vibrational state by REMPI and then dissociated into fragments, which can be velocity-mapped onto the two-dimensional imaging detector directly by a second photolysis laser or another photon from the same laser.[9]

The main advantage of these techniques is that the resulting images directly allow for the extraction of the velocity and angular distribution of the fragments, providing insight into the photofragmentation dynamics of molecular ions. For complex molecules, multiple dissociation channels may exist, and it can be cumbersome to record them all and measure branching between them accurately. Ni and co-workers recently pioneered the development of a multimass imaging technique to detect many different fragments for large molecules simultaneously by using a constant-momentum mass spectrometer with a two-dimensional imaging detector in conjunction with VUV photoionization.[10] This approach provides speed distributions for multiple masses simultaneously, but not precise branching or the angular distributions. We have recently developed a versatile reflectron velocity map imaging apparatus that can be employed in a multimass configuration to obtain the full velocity distributions and branching fractions for multiple masses simultaneously.

The ethylene cation represents a prototyical system in the study of electronic relaxation mechanisms and the influence of conical intersections on dissociation dynamics, both experimentally[11−15] and theoretically.[16−18] The thresholds for H and H_2 elimination from $C_2H_4^+$ ($\tilde{X}\ ^2B_{3u}$) are very close in energy, and they exhibit different correlations to the electronic states involved in the dissociation. The competition between them can thus provide insight into the complex couplings among these numerous cation electronic states that are accessible at modest excitation energies.

In the present communication, we briefly report use of a new experimental approach, reflectron multimass velocity map ion imaging, to explore the state-selected photodissociation of $C_2H_4^+$ ions. The approach employs state preparation by well-defined two-photon resonant, three-photon ionization via vibronic bands of (π, nf) Rydberg states in the vicinity of the ionization potential

* Corresponding author. E-mail: asuits@chem.wayne.edu.
† Wayne State University.
‡ SUNY Stony Brook.

10.1021/jp053143m CCC: $30.25

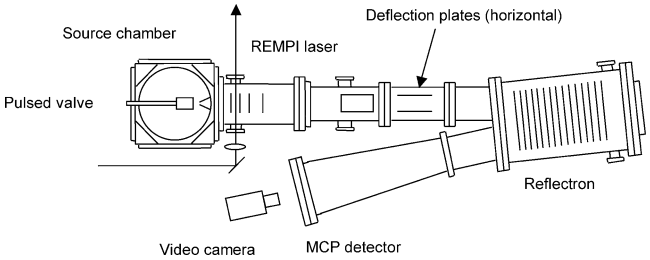

Figure 1. Schematic view of the reflectron multimass velocity map ion imaging apparatus.

(10.517 eV)[11] of ethylene. The $C_2H_4^+$ ions subsequently undergo photodissociation through the $\tilde{B}\ ^2A_g$ state by absorption of another photon. In this approach, we simultaneously record images of photofragment $C_2H_3^+$ and $C_2H_2^+$ ions and directly obtain the velocity distribution and branching fraction ratios for these competitive dissociation pathways.

The reflectron multimass velocity map ion imaging apparatus used in this study, shown in Figure 1, will be described in more detail elsewhere,[20] and only a brief sketch is given here. The apparatus consists of a source chamber, a reaction chamber with ion optics and two orthogonal sets of deflection plates, a single stage reflectron, and an MCP/phosphor detector. A pulsed supersonic molecular beam of ethylene (Linde, CP Grade, 99.5%) is made by expanding ethylene molecules diluted to about 5% with argon at a backing pressure of 1.5 bar from a piezoelectric pulsed nozzle having a 1-mm orifice into the source chamber of our differentially pumped apparatus. After passing through a 1-mm-diameter skimmer located 3.8 cm downstream of the pulsed nozzle orifice, then a 2-mm collimator, the supersonic molecular beam enters into a velocity mapping ion optics assembly consisting of four electrodes. The molecular beam is perpendicularly intersected with a laser beam tuned to a two-photon resonant excitation of Rydberg states of ethylene. The operating pressures were maintained at $\sim 2.5 \times 10^{-5}$ Torr in the source chamber and at $\leq 1 \times 10^{-7}$ Torr in the main chamber. The laser light in the present study was generated by sum-frequency mixing the third harmonic of an injection-seeded Nd:YAG laser with the output of a dye laser (Sirah, LDS720 dye) pumped by the second harmonic of the same Nd:YAG laser (Spectra-physics, Quanta-Ray). The laser beam was vertically polarized, parallel to the detector surface, then focused with a lens ($f = 20$ cm) into the interaction volume with the pulsed molecular beam. Typical output power for the pulsed dye laser beam entering chamber was 1−1.5 mJ/pulse, spanning a wavelength range from 240 to 242 nm, and accurate wavelength calibration was achieved using a wavemeter (Coherent WaveMaster).

In these experiments, a single laser was used to ionize the C_2H_4 by two-photon resonant, three-photon ionization via the (π, nf) Rydberg states and to photodissociate the resulting $C_2H_4^+$ ions. Both ionization and dissociation occur within the same laser pulse. On the basis of previous assignments by Cool and co-workers,[19] the laser wavelengths were carefully tuned to 241.0684 nm (in vacuum; two-photon, 82 964 cm^{-1}) corresponding to the $7f\ 4_0^2$ vibronic band and 240.7782 nm (in vacuum; two-photon, 83 064 cm^{-1}) corresponding to the $8f\ 0_0^0$ vibronic band. The ion signal was negligible when the laser was tuned slightly off-resonance. Although we have not examined the photoelectron spectra to ensure that we have achieved strict vibrational-state preparation on these transitions, we have examined this in the analogous 3s Rydberg states. As expected, we find nearly pure vertical ionization from the prepared Rydberg state except when combination bands are excited. Following ionization and dissociation, the photofragments are accelerated through the multilens velocity mapping assembly up to a kinetic energy of 5 kV. After passing through a field-free region, the ion packets enter into a region with two plates of opposite polarity located 635 mm downstream from the interaction volume. The plates were then pulsed to ±225 V for 240-ns duration in order to separate the ions of different masses spatially according to mass-to-charge ratio. The ions then enter a single-stage reflectron consisting of a stack of 36 electrodes. In this region, the ions turn around because of the retarding field of the reflectron and are then reaccelerated toward a detector through another field-free region. The ions of different masses finally impact upon a position-sensitive dual MCP/P-47 phosphor screen of 120-mm diameter (Burle). A high-voltage pulse of 1.2 μs in duration was applied to the MCP for the time gate of the $C_2H_4^+$, $C_2H_3^+$, and $C_2H_2^+$ ions at the same time, and the resulting image was recorded using a CCD camera (Mintron 2821e) in conjunction with PC acquisition software (McLaren Research), which permitted real-time event-counting of the data. The signals were typically accumulated for 40 000 laser shots for each data set. The calibration of our images was achieved on the basis of the image of CO ($v = 0$, $J = 65$) probed by REMPI that we observed experimentally in the photodissociation of OCS at 230 nm, while all apparatus parameters were kept the same.

Experimental velocity-mapped images from the state-selected photodissociation of $C_2H_4^+$ following excitation into the $\tilde{B}\ ^2A_g$ state recorded using reflectron multimass velocity map ion imaging are shown in Figure 2A,B, respectively. The linearly polarized light is vertical in the plane of the figure. In both cases, the three images mapped on the detector plane are spatially separated along the horizontal axis according to mass-to-charge ratio, clearly showing the simultaneous mass and kinetic energy multiplexing capability of the instrument. In these images, the right image (a blurred spot) of weak intensity is easily assigned to the parent $C_2H_4^+$ ($m/e = 28$) ions that have virtually no recoil velocity; the next two adjacent images can be assigned to $C_2H_3^+$ ($m/e = 27$) and $C_2H_2^+$ ions ($m/e = 26$) originating from the photodissociation of $C_2H_4^+$ ($m/e = 28$) at 241.0684 nm (Figure 2A) and 240.7782 nm (Figure 2B). Thus, it is immediately apparent from the relative intensities among the different masses in the two images that most of the initially formed $C_2H_4^+$ ions undergo photofragmentation and the H elimination channel is much more favorable than the H_2 channel, consistent with the previous studies of the same energy range obtained by single-photon photoionization mass spectrometry and threshold photoelectron−photoion coincidence (TPEPICO) spectroscopy.[11,13] Although the photofragment images for $C_2H_3^+$ and $C_2H_2^+$ show broad features without any distinct structure, one particularly interesting result is that a subtle difference in the signal intensity is visible between two $C_2H_2^+$ images under careful inspection, suggesting that it may be correlated to the initial vibrational-state preparation of the parent $C_2H_4^+$ ion before the photodissociation event takes place. The image for $C_2H_2^+$ corresponding to the $8f\ 0_0^0$ origin band excitation is also slightly larger than that for the $7f\ 4_0^2$ torsional band excitation.

These images are two-dimensional projections of the recoiling $C_2H_3^+$ and $C_2H_2^+$ velocity distributions, and the three-dimensional distributions were reconstructed by Vrakking's iterative inversion technique.[21] The total translational energy distributions were then obtained by the appropriate integration of the slice through the three-dimensional distribution. These are shown in Figure 3A,B for the two dissociation channels at

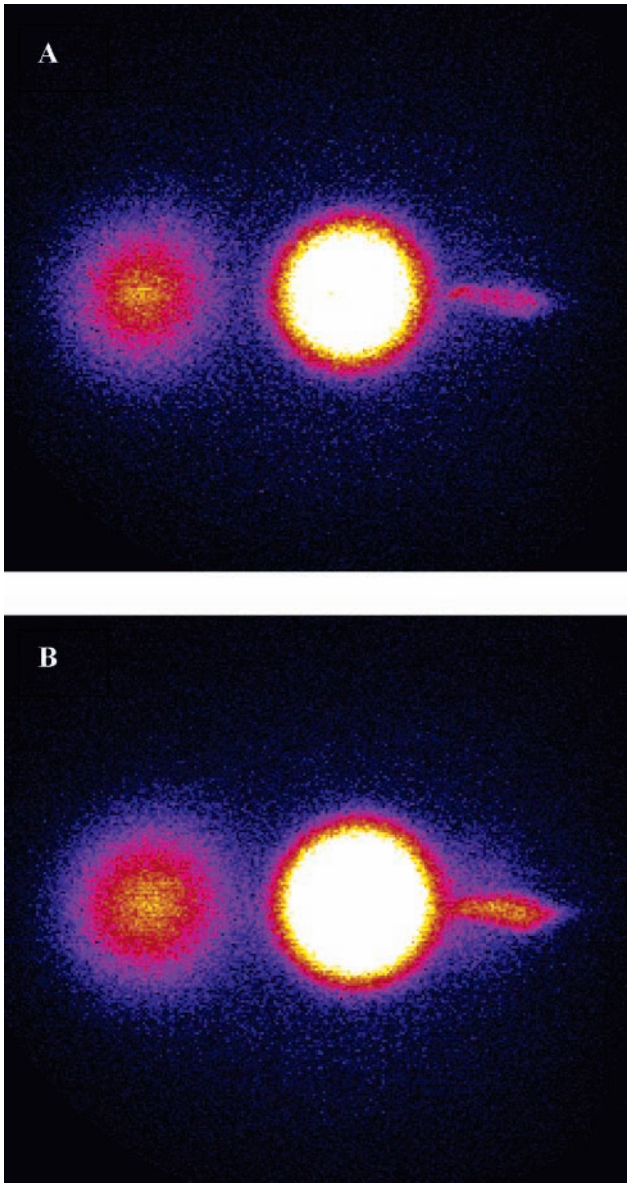

Figure 2. Experimental photofragment images from the photodissociation of $C_2H_4^+$ produced by two-photon resonant, three-photon ionization via vibronic bands of (π, nf) Rydberg states, $7f\,4_0^2$ (A) and $8f\,0_0^0$ (B), respectively. The laser polarization was vertical in the plane of the figures.

the different excitation energies. The total translational energy distributions generally peak close to zero energy and roughly exponentially decay to higher energy, suggesting a statistical dissociation process.[22] As summarized in Table 1, the average total translational energies of the H elimination channels are $\langle E_T \rangle = \sim 0.40$ eV for $8f\,0_0^0$ origin band excitation and $\langle E_T \rangle = \sim 0.37$ eV for $7f\,4_0^2$ torsional band excitation. In case of the H_2 elimination channels, the average translational energy release was $\langle E_T \rangle = \sim 0.35$ eV for $8f\,0_0^0$ origin band excitation and $\langle E_T \rangle = \sim 0.30$ eV for $7f\,4_0^2$ torsional band excitation. When exciting through the origin band, the H_2 elimination channel displayed slightly higher recoil energy when compared to that of the torsion-excited band, even though there is less available energy. Although the difference in average translational energy between the torsion-excited and origin excitation is only marginally significant, the key result, as illustrated in Figure 3A, is the substantial difference in branching ratios between the H and H_2 elimination channels with vibrational excitation.

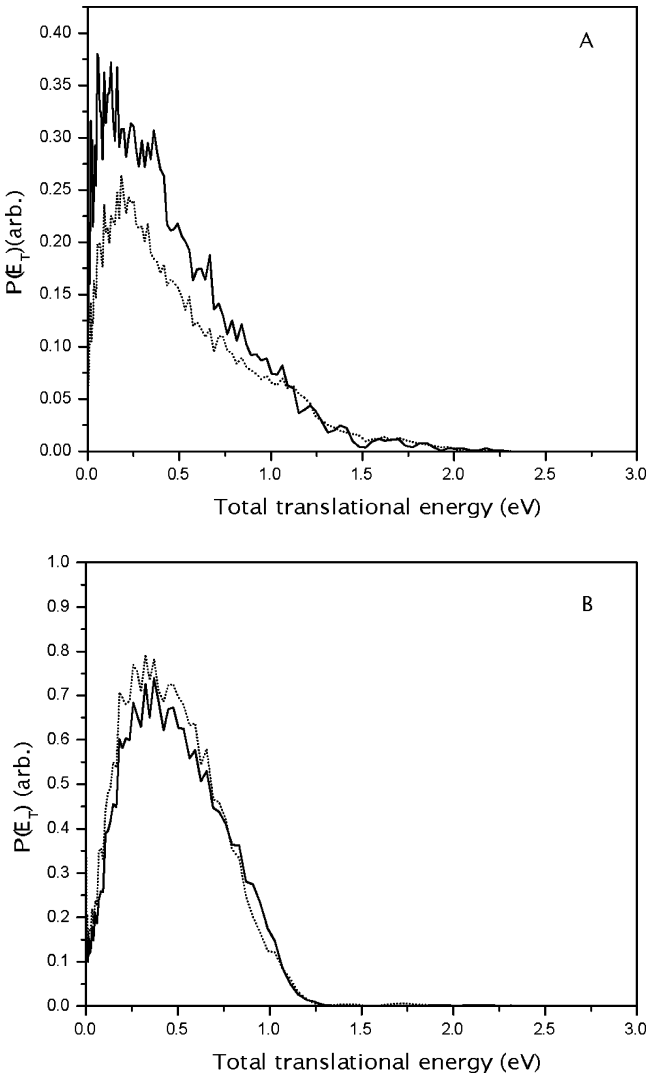

Figure 3. The total translational energy distributions for both H_2 (A) and H (B) elimination channels obtained from the images in Figure 2A,B. The solid lines correspond to the $7f\,4_0^2$ torsional band excitation, and the dotted lines correspond to the $8f\,0_0^0$ origin band excitation. The distributions are scaled so that the total integrals for each transition are equal. The branching ratios are thus directly reflected in the $P(E)$'s.

TABLE 1: Values Obtained from Image Analysis for Two Different Vibronic Excitations

parameter	$8f\,0_0^0$ origin band	$7f\,4_0^2$ torsional band
wavelength (λ/nm)	240.7782	241.0684
E_{avail} (eV)	2.44 ($C_2H_3^+$)	2.49 ($C_2H_3^+$)
	2.52 ($C_2H_2^+$)	2.57 ($C_2H_2^+$)
$\langle E_T \rangle$ (eV)	0.40 ± 0.03 ($C_2H_3^+$)	0.37 ± 0.04 ($C_2H_3^+$)
	0.35 ± 0.03 ($C_2H_2^+$)	0.30 ± 0.03 ($C_2H_2^+$)
branching ratios ($C_2H_3^+$:$C_2H_2^+$)	3.82:1.00 (±0.22)	2.84:1.00 (±0.20)

The energies relative to the cation ground state for the two competing dissociation channels in this experiment are shown below:

$$C_2H_4(\tilde{X}\ ^1A_g) \xrightarrow{2h\nu} C_2H_4^*(7f\,4_0^2,\ 8f\,0_0^0) \xrightarrow{h\nu} C_2H_4^+(\tilde{X}\ ^2B_{3u}) \xrightarrow{h\nu}$$

$$C_2H_4^{+*}(\tilde{B}\ ^2A_g) \rightarrow C_2H_3^+ + H \qquad 2.62\ (\pm 0.01)\ \text{eV} \quad (1)$$

$$\rightarrow C_2H_2^+ + H_2 \qquad 2.70\ (\pm 0.02)\ \text{eV} \quad (2)$$

Assuming that the initial vibrational states in the ground electronic ionic state of $C_2H_4^+(\tilde{X}\ ^2B_{3u})$ prepared by REMPI are

a two-quanta torsional-mode (ν_4) excitation ($2\nu_4 = 438.2$ cm^{-1})[14] and a vibrationless state, the available energies are 2.49 ($C_2H_3^+$) and 2.57 ($C_2H_2^+$) eV for $7f\ 4_0^2$ torsional-band excitation and 2.44 ($C_2H_3^+$) and 2.52 ($C_2H_2^+$) eV for $8f\ 0_0^0$ origin-band excitation based on the above reference values of the dissociation energy for two channels obtained by Stockbauer and Inghram.[11] Therefore, the measured average total translational energies account for only 12−16% of the available energy. The lower average translational energy values for the H_2 elimination channel may be partly a consequence of the energy partitioning into H_2 internal modes. The $C_2H_3^+$:$C_2H_2^+$ branching ratios obtained by direct integration of the images are (2.84 ± 0.20):1.00 for $7f\ 4_0^2$ torsional-band excitation and (3.82 ± 0.22):1.00 for $8f\ 0_0^0$ origin-band excitation, respectively. While the latter value is reasonably consistent with the TPEPICO result[11] at the same energy, approximately 4.00:1.00, the former value indicates that the $C_2H_2^+$ channel is enhanced with torsional excitation. These results suggest that, although the two vibronic excitation wavelengths are very close to each other, the vibrational-state selection of the ground electronic state $C_2H_4^+$ ($\tilde{X}\ ^2B_{3u}$) may have significant impact on the dissociation pathways for the two competing channels.

The central questions raised by the results presented here are the nature of the dissociation mechanism of $C_2H_4^+$ in its $\tilde{B}\ ^2A_g$ electronically excited state and the mechanism for the enhanced branching to the H_2 elimination following torsional excitation in the ground state prior to photodissociation. Following symmetry selection rules, the transition from the ground state of $C_2H_4^+$ ($\tilde{X}\ ^2B_{3u}$) to the $\tilde{B}\ ^2A_g$ electronically excited state is allowed for single-photon excitation, although to our knowledge, this process has not been studied directly before. An alternative interpretation of the present results is that some structure in the $\tilde{B}\ ^2A_g$ dissociation continuum gives rise to the wavelength dependence we observe. According to a previous photoelectron study,[12] the $\tilde{B}\ ^2A_g$ state is mostly featureless at the energies employed herein, with some poorly resolved vibrational structure appearing for lower energies. The latter has been assigned to a progression in the C−C stretching (ν_2) and CH_2 scissors modes (ν_3). In addition, the edge of the $\tilde{C}\ ^2B_{2u}$ state lies in this region, further complicating the spectrum. Given these considerations, we find it less likely that mode-selective dissociation is taking place in this system. The $\tilde{B}\ ^2A_g$ excited state is believed[11,12,16,17] to undergo rapid internal conversion to the vibrationally excited electronic ground state $\tilde{X}\ ^2B_{3u}$, through the $\tilde{C}\ ^2B_{2u}$ state (which correlates to the ground-state molecule for 180° rotation about the C−C bond) or through the $\tilde{A}\ ^2B_{3g}$ state. Lorquet and coworkers pointed out from theoretical considerations for the photodissociation from the $\tilde{B}\ ^2A_g$ excited state that the $C_2H_2^+$ channel can proceed adiabatically on the ground state by the transformation into an isomerized ethylidene (CH_3CH^+) structure. On the other hand, the $C_2H_3^+$ channel requires electronic coupling to the $\tilde{A}\ ^2B_{3g}$ state through excitation of the torsional vibration around the conical intersection along the C−H stretching coordinate (ν_1), correlating asymptotically to the lowest dissociation pathway, $C_2H_3^+ + H$.[16,17]

We might reasonably anticipate that any state-selective behavior would be washed out in the photodissociation of $C_2H_4^+$ following $\tilde{B}\ ^2A_g$ excitation, owing to the extensive rearrangements occurring on the ground state, with the branching ratios ultimately depending only on the total internal energy of the system.[17] However, torsional excitation can have a profound effect on the Franck−Condon-mediated access to various configurations of the $\tilde{B}\ ^2A_g$ state, which may then strongly influence relative access to the ground state and the $\tilde{A}\ ^2B_{3g}$ state, or perhaps simply determine the regions of these surfaces that are accessed following internal conversion. This may be because, for the ground state of the cation, the torsion angle is constrained to 27° and planar geometries are not accessed. Two quanta of torsional excitation takes the system above the barrier to planarity, so that entirely different regions of the $\tilde{B}\ ^2A_g$ state may be accessed. This may then profoundly alter the internal conversion from the $\tilde{B}\ ^2A_g$ state to the $\tilde{A}\ ^2B_{3g}$ state, the $\tilde{C}\ ^2B_{2u}$ state, and the ground state. Thus, the present preliminary results suggest a number of future experimental and theoretical studies such as photoelectron imaging, further vibrationally mediated photodissocition studies, and especially dynamical calculations involving the excited-state potential surfaces and nonadiabatic interactions. This work is underway.

Acknowledgment. We would like to acknowledge Shen Lei, Wen Li, and S. A. Lahankar for their helpful assistance. This work was supported by the National Science Foundation under award number CHE-0415393.

References and Notes

(1) Crim, F. F. *Acc. Chem. Res*. **1999**, *32*, 877.
(2) Chiu, Y.; Yang, B.; Fu, H.; Anderson, S. L.; Schweizer, M.; Gerlich, D. *J. Chem. Phys*. **1992**, *96*, 5781.
(3) Eppink, A. T. J. B.; Parker, D. H. *Rev. Sci. Instrum.* **1997**, *68*, 3477.
(4) Gebhardt, C. R.; Rakitzis, T. P.; Samartzis, P. C.; Ladopoulos, V.; Kitsopoulos, T. N. *Rev. Sci. Instrum.* **2001**, *72*, 3848.
(5) Townsend, D.; Minitti, M. P.; Suits, A. G. *Rev. Sci. Instrum.* **2003**, *74*, 2530.
(6) Chang, C.; Luo, C. Y.; Liu, K. *J. Phys. Chem. A* **2005**, *109*, 1022.
(7) Beckert, M.; Greaves, S. J.; Ashfold, M. N. R. *Phys. Chem. Chem. Phys.* **2003**, *5*, 308.
(8) Aguirre, F.; Pratt, S. T. *J. Chem. Phys.* **2003**, *118*, 6318, 9467.
(9) Nahler, N. H.; Vieuxmaire, O. P. J.; Jones, J. R.; Eppink, A. T. J. B.; Coriou, A. M.; Parker, D. H.; Ashfold, M. N. R. *J. Phys. Chem. A* **2004**, *108*, 8077.
(10) Tsai, S.; Lin, C.; Lee, Y. T.; Ni, C. *Rev. Sci. Instrum.* **2001**, *72*, 1963.
(11) Stockerbauer, R.; Inghram, M. G. *J. Chem. Phys*. **1975**, *62*, 4862.
(12) Pollard, J. E.; Trevor, D. J.; Reutt, J. E.; Lee, Y. T.; Shirley, D. A. *J. Chem. Phys*. **1984**, *81*, 5302.
(13) Mackie, R. A.; Scully, S. W. J.; Sands, A. M.; Browning R.; Dunn, K. F.; Latimer, C. J. *Int. J. Mass Spectrom.* **2003**, *223*, 67.
(14) Willitsch, S.; Hollenstein, U.; Merkt, F. *J. Chem. Phys*. **2004**, *120*, 1761.
(15) Wang, P.; Xing, X.; Baek, S. J.; Ng, C. Y. *J. Phys. Chem. A* **2004**, *108*, 10035.
(16) Scannen, C.; Raseev, G.; Galloy, C.; Fauville, G.; Lorquet, J. C. *J. Chem. Phys*. **1981**, *74*, 2402.
(17) Desouter-Lecomte, M.; Scannen, C.; Lorquet, J. C. *J. Chem. Phys*. **1983**, *79*, 894.
(18) Luis, J. M.; Torrent-Sucarrat, M.; Sola, M.; Bishop, D. M.; Kirtman, B. *J. Chem. Phys*. **2005**, *122*, 184104.
(19) Williams, B.; Cool, T. A. *J. Chem. Phys*. **1991**, *94*, 6358.
(20) Leskiw, B. D.; Kim, M. H.; Suits, A. G. *Rev. Sci. Instrum*. (submitted).
(21) Vrakking, M. J. J. *Rev. Sci. Instrum.* **2001**, *72*, 4084.
(22) Klots, C. E. *J. Chem. Phys*. **1976**, *64*, 4269.